Journal of Alloys and Compounds 900 (2022) 163416

Contents lists available at ScienceDirect

Journal of Alloys and Compounds

journal homepage: www.elsevier.com/locate/jalcom

Ferromagnetic resonance line broadening and shift effect in nanocrystalline thin magnetic films: Relation with crystalline and magnetic structure

A.V. Izotov[a,b,*], B.A. Belyaev[a,b], N.M. Boev[a,b], A.V. Burmitskikh[a,b], G.V. Skomorokhov[b], S.M. Zharkov[a,b], P.N. Solovev[b,**]

[a] Siberian Federal University, 79 Svobodny pr., Krasnoyarsk 660041, Russia
[b] Kirensky Institute of Physics, Federal Research Center KSC SB RAS, 50/38 Akademgorodok, Krasnoyarsk 660036, Russia

ARTICLE INFO

Article history:
Received 20 September 2021
Received in revised form 2 December 2021
Accepted 22 December 2021
Available online 27 December 2021

Keywords:
Nanocrystallite
Magnetization ripple
Ferromagnetic resonance (FMR)
Two-magnon scattering process
Micromagnetic simulation

ABSTRACT

With the rapid development of telecommunication technologies and highly integrated electronic devices, researchers show great interest in nanocrystalline soft magnetic thin films with unique characteristics for microwave applications. An important direction of the current research in this field is the study of high-frequency magnetization dynamics that directly depends on the damping processes in a magnetic medium. This paper reports on the effect of sharp broadening and shift of the ferromagnetic resonance (FMR) line revealed experimentally in a 40-nm-thick nanocrystalline permalloy ($Fe_{20}Ni_{80}$) thin film at a frequency of about 5 GHz. The effect arises only in films with crystallite size exceeding some critical value D_{cr}. The micromagnetic simulation demonstrates that exchange and dipolar interactions between randomly oriented crystallites form in the film a quasiperiodic magnetic structure with a characteristic wavelength in the range from 36 nm to 3.3 μm. An analysis of the two-magnon scattering model and simulation results shows that the formed magnetic structure provides the energy transfer from uniform magnetization oscillations (uniform FMR) to spin waves, which results in an additional energy dissipation channel and, consequently, sharp FMR line broadening. A theoretical estimate of the critical crystallite size D_{cr} based on this model yields a value of ~14.3 nm for 40-nm-thick $Fe_{20}Ni_{80}$ films.

1. Introduction

The rapid development of telecommunication and information technologies poses new, increasingly more complicated challenges for the developers and designers of modern microelectronic devices. With the explosive growth of mobile data traffic and the amount of processed data, the relevance of mastering higher operating frequencies of the microwave range is dramatically increasing. At the same time, current trends in the development of electronic devices focus on miniaturization and integration. Magnetic materials are one of the main components of most microwave devices. Compared with ferrites traditionally used in microwave technology [1], nanocrystalline soft magnetic materials such as alloys of FeCuNbSiB [2], FeBNbCu [3], FeZrB (Cu) [4], FeCo [5], and FeNi [6] have larger saturation magnetization, higher magnetic permeability, and lower eddy current losses, making them more appealing for microwave applications.

Thin nanocrystalline soft magnetic films and multilayer structures attract special interest due to their prospects in modern technological applications [7]. On the one hand, such structures can be effectively used in devices compatible with planar technology. On the other hand, the use of nanocrystalline thin-film magnetic structures instead of bulk materials allows to substantially increase the magnetic permeability of the medium and shift its operating frequency range towards higher frequencies [8,9]. Acher's constraint on the microwave permeability and the FMR frequency of magnetic composites demonstrates a clear advantage of thin-film magnetic materials in comparison with their bulk counterparts [9,10]. Additionally, thin-film structures make it possible to choose the composition of a nanocrystalline alloy more flexibly and apply different synthesis technologies [11].

* Corresponding author at: Siberian Federal University, 79 Svobodny pr., Krasnoyarsk 660041, Russia.
** Corresponding author.
E-mail addresses: aizotov@sfu-kras.ru (A.V. Izotov), psolovev@iph.krasn.ru (P.N. Solovev).

https://doi.org/10.1016/j.jallcom.2021.163416
0925-8388/

From the viewpoint of microwave applications, the ferromagnetic resonance linewidth is one of the most (if not the most) important parameters that directly characterize damping in magnetic medium [12]. First of all, the FMR linewidth of any magnetic material depends on its intrinsic damping parameter. At the same time, there are additional extrinsic mechanisms of magnetization relaxation, among which the two-magnon scattering processes give a dominant contribution to the microwave power absorption and FMR line broadening of thin magnetic films [13]. These processes are caused by the damping of spin waves (magnons) when they interact with nonuniform internal magnetic fields arising in a magnetic material due to various reasons. In particular, the effect of the random local anisotropy on the two-magnon scattering processes of polycrystalline thin films has been studied in Ref. [14,15], and the effect of randomly distributed roughnesses on the surface of the film has been addressed in Ref. [16,17]. Also, the possibility of controlling the magnetic damping in films by introducing artificial magnetic inhomogeneities has been more recently reported in several papers [18–20].

Studies of nanocrystalline thin films have revealed a strong effect of the crystallite size on the coercivity, magnetic anisotropy and permeability of the films [21,22]. If the crystallite size is less than the magnetic correlation length, the exchange and dipolar interactions between crystallites average out the random anisotropy of individual crystallites, which leads to a substantial decrease in the coercivity and an increase in the permeability of the nanocrystalline medium. This also results in an emergence of a unique wavelike quasiperiodic magnetic structure, which wavelength depends on magnetic parameters of the film and the strength of an applied magnetic field [23–26]. This nonuniform magnetic structure, called magnetization ripple, might be the source of additional damping mechanisms in thin films [27,28].

In this paper, we investigate the revealed in nanocrystalline permalloy thin film effect of the sharp broadening and shift of the FMR line, caused by the scattering of spin waves on the quasiperiodic magnetic structure – magnetization ripple. The possibility of the existence of this effect was first pointed out by Ignatchenko and Degtyarev [29] and more recently using the micromagnetic simulation by the authors of the present study [30]. For a detailed exploration of the effect, the results of structural and magneto-structural studies, as well as the results of scanning and broadband FMR spectroscopy, were supplemented by the results of micromagnetic simulations of the magnetic structure and high-frequency magnetic permeability of the films. To explain the physical mechanism of the effect, we also considered the two-magnon scattering model with which we derived an expression for estimating the critical crystallite size below which the effect disappears.

2. Experimental

2.1. Samples synthesis

Two nanocrystalline thin magnetic films (sample 1 and sample 2) with thicknesses of 40 nm were simultaneously fabricated in one deposition cycle by DC magnetron sputtering of $Fe_{20}Ni_{80}$ target (Kurt J. Lesker Company). The films were deposited on quartz glass 12 × 12 × 0.5 mm^3 size substrates having a roughness of 1 nm or so. Before the sputtering, the substrates were washed in an ultrasonic bath in a hot weak soap solution and 10% H_2O_2 solution, followed by drying in isopropyl alcohol vapor. After the washing procedure, an amorphous SiO layer with a thickness of 200 nm was thermally deposited on the substrates to exclude the possibility of large crystallites formation on the initial stage of magnetic film growth. The substrates were placed in the substrate holder with a square mask 10 × 10 mm^2 in size. The distance between the target and the substrates was 170 mm. The magnetron power density near the target was kept constant at 4.7 W/cm^2, which provided a deposition rate of 0.25 nm/s. The base pressure was 3×10^{-4} Pa, and the argon pressure during magnetron sputtering was 2×10^{-1} Pa. The temperature of the substrates was maintained at 200 °C, and a uniform static magnetic field of 200 Oe was applied in the films plane to induce uniaxial magnetic anisotropy. After the sputtering, sample 1 was removed from the vacuum chamber, while sample 2 was left to be annealed (to induce crystallites growth) at a temperature of 350 °C for 3 h. During the annealing, the pressure was 3×10^{-4} Pa, and the same static field of 200 Oe was applied to the sample.

2.2. Characterization of crystalline and magnetic structure

The morphology, microstructure and local elemental composition of the samples were characterized by transmission electron microscopy (TEM) using a JEM-2100 (JEOL Ltd.) microscope operating at the accelerating voltage of 200 kV. The microscope was equipped with an energy dispersive spectrometer (EDS), Oxford Inca x-sight, which was used to determine the elemental composition of the samples. The selected area electron diffraction (SAED) and high-resolution TEM (HRTEM) were employed to determine the structure of the crystallites. The magnetic structure of thin films was imaged by Lorentz transmission electron microscopy (Lorentz TEM) [31,32] using a JEM-2100 (JEOL Ltd.) electron microscope. For TEM measurements, magnetic films were preliminarily separated from substrates using a 10% aqueous solution of hydrofluoric acid and placed on Cu TEM support grids.

2.3. Microwave measurements

The microwave magnetic properties of the samples were investigated using a shorted microstrip line fixture connected to a vector network analyzer (VNA) R&S ZNB20. The design of the fixture, inside which the sample was placed, and the overall scheme of the measurement setup used in this work were analogous to those presented in Ref. [33]. The frequency band of the measurement setup was ranged from 100 MHz to 9.5 GHz. The measurements were carried out in the frequency sweep mode for in-plane static magnetic field values ranging from 0 to 1 kOe. The complex magnetic permeability of the films $\mu = \mu' - i\mu''$ was determined from the scattering matrix component S_{11}, which characterizes the reflection of the microwave signal from the fixture. For this, we used an analytical expression (6) of Ref. [34]. Before each measurement, the setup was calibrated by subtracting the background signal (including the signal from the substrate) from the total one. This was achieved by applying an external magnetic field and saturating the investigated film along the direction parallel to the microwave field. In this case, the magnetic response from the film vanished, and the background output signal was used to calibrate the VNA. After that, the permeability μ was measured in a magnetic field H applied perpendicularly to the microwave field, when the maximum magnetic response from the film was expected.

The basic magnetic properties of the samples were determined using a scanning FMR spectrometer [35,36]. The absorption spectra were measured at a fixed driving frequency of 2.5 GHz while sweeping an in-plane magnetic field. The effective saturation magnetization M_{eff} and the value of the in-plane uniaxial magnetic anisotropy field H_u were extracted from the measured angular dependencies of the resonance field by fitting the parameters of a theoretical model of a single domain film to the experimental data [37,38]. It should be noted that the FMR method allows for the determination of not the actual saturation magnetization M_s of the films but only its effective value $M_{eff} = M_s - H_p/4\pi$. The perpendicular magnetic anisotropy H_p in this expression can be related to the surface anisotropy of the films [11], or nonuniform magnetic fields originated, for instance, from columnar microstructure formed in

the films [39,40] or roughnesses on the film substrate [41]. Usually, $H_p << 4\pi M_s$, and it can be considered approximately that $M_{eff} \approx M_s$.

All experiments presented in this paper were performed at room temperature.

2.4. Simulation details

We numerically investigated the magnetic microstructure and the microwave permeability of nanocrystalline thin films using a micromagnetic model, which justification and detailed description are given in Refs. [30,42,43]. The model is based on the following expression for the free energy of the nanocrystalline thin magnetic film:

$$F = \int_V \left[-\mathbf{H}\cdot\mathbf{M} + \frac{A}{M_s^2}(\nabla\mathbf{M})^2 - \frac{1}{2}\mathbf{H}^m\cdot\mathbf{M} - \frac{K_u}{M_s^2}(\mathbf{M}\cdot\mathbf{n})^2 - \frac{K}{M_s^2}(\mathbf{M}\cdot\mathbf{l})^2 \right] dV. \quad (1)$$

Here, the first term describes the energy of an external magnetic field **H** (the Zeeman energy), the second – the energy of the exchange interaction with the exchange stiffness constant A, the third – the energy of the demagnetizing field $\mathbf{H}^m$ (the dipolar interaction), and the fourth – the induced uniaxial magnetic anisotropy with the constant K_u and easy axis unit vector **n**. The last term of the expression represents the energy of the local uniaxial magnetic anisotropy K with a random orientation of easy axes in the crystallites $\mathbf{l} = \mathbf{l}(\mathbf{r})$. We note that the usage of uniaxial symmetry instead of cubic one for the description of the random magnetic anisotropy in the model makes it possible to significantly simplify the calculations and reduce the computation time. Moreover, as shown in Refs. [23–26], due to the averaging of the random anisotropy the influence of its symmetry results only in the renormalization of local anisotropy constant, in particular, in the substitution in (1) of K for $0.39K_1$, where K_1 is the constant of local cubic anisotropy (see, for example, Appendix B in Ref. [25]). The distribution of the magnetization is described by the vector $\mathbf{M}(\mathbf{r})$, the modulus of which is constant $|\mathbf{M}(\mathbf{r}, t)| = M_s$. The demagnetizing field $\mathbf{H}^m$ was determined from the magnetostatic approximation of the Maxwell equations $\mathrm{rot}(\mathbf{H}^m) = 0$ and $\mathrm{div}(\mathbf{H}^m) = -4\pi\ \mathrm{div}(\mathbf{M})$ [43], using analytical expressions of Ref. [44].

Using the finite-difference method [42], the considered object was discretized on N identical cuboid elements of volume V_0, where the magnetization vector $\mathbf{M}_i$, ($i = 1,2,..,N$) was constant within each element. The in-plane size of the elements equaled the average crystallite size D_0, while the height of the elements equaled the thickness of the film, that is $V_0 = D_0^2 d$. The total number of the discrete elements in the film plane xy was $N = Nx \times Ny = 2048 \times 2048 \approx 4 \times 10^6$. Two-dimensional periodic boundary conditions were applied to the dipolar and exchange interactions [45], to exclude the influence of the internal magnetic field inhomogeneity arising at the edges of finite-size samples [46].

The magnetic microstructure (equilibrium distribution of the magnetization $\mathbf{M}_i$) of nanocrystalline thin films was determined from the solution of the system of linear inhomogeneous equations with undetermined Lagrange multipliers [42]. Each equilibrium magnetization distribution was tested for stability. In the case of instability of the obtained solution, the search for a new equilibrium state in the direction of the system relaxation was made [42]. The microwave magnetic permeability of the films was calculated by the method of undetermined coefficients for solving the system of linearized Landau–Lifshitz equations [43], describing the magnetization oscillation in each discrete element.

3. Results and discussion

3.1. Composition and crystalline structure

Fig. 1a–c displays the results of transmission electron microscopy and electron diffraction investigations for sample 1, and Fig. 1d–f for annealed at 350 °C sample 2. As can be seen, the as-deposited film (sample 1) has a nanocrystalline structure (Fig. 1a). The electron diffraction pattern (inset in Fig. 1a) obtained for the film area 1.3 μm in diameter indicates that the crystallites are randomly oriented. These close-packed crystallites with sizes ranging from 4 to 28 nm comprise the continuous film. The crystallite size distribution obtained from the analysis of the TEM images of sample 1 has an almost symmetrical shape and can be well described by a normal distribution with the mean value D_0 = 11.6 nm and the standard deviation σ = 3.4 nm (Fig. 1c). As Fig. 1d–f evidence, the annealing of sample 2 at 350 °C for 3 h expectedly resulted in the crystallite size growth. The crystallite diameter spreads substantially, from 4 to 150 nm, with the mean value D_0 = 40.1 nm and the standard deviation σ = 22.1 nm. In contrast to as-deposited sample 1, the crystallite size distribution of annealed sample 2 is asymmetrical (Fig. 1f) and more consistent with a log-normal distribution, which is commonly observed for polycrystalline materials [47]. The EDS data show that for both samples 1 and 2, the atomic percentage of Fe was 20 ± 0.5 at%, and Ni 80 ± 0.5 at%. An analysis of the SAED patterns and HRTEM images also indicates that the films consist of $Fe_{20}Ni_{80}$ crystallites (space group Fm-3m, lattice constant a = 0.355 nm). The SAED patterns (Fig. 1a, d) demonstrate the full set of diffraction reflections of a polycrystalline type that correspond to the face-centered cubic crystal structure of $Fe_{20}Ni_{80}$. The results of structural analysis and elemental composition data for samples 1 and 2 are summarized in Table 1.

3.2. Magnetic structure

Fig. 2 presents images of the magnetic structure typical for sample 1 (Fig. 2a, b) and sample 2 (Fig. 2d, e) obtained by Lorentz TEM without an external magnetic field in the film region. The contrast in Lorentz TEM images arises due to the interaction of electrons with the magnetization of the film and their deflection when passing through the sample [31,32]. A low-angle Néel domain wall network is clearly distinguished for sample 1 (Fig. 2a, b), visible on the image as high-contrast bright and dark lines, depending on the orientation of the magnetization on both sides of the walls. Furthermore, magnetic imaging shows that the magnetization orientation varies even inside the magnetic domain, which can be seen on the image as thin bright and dark wavelike lines that are perpendicular to the direction of the local magnetization **M**. This fine magnetic structure known as magnetization ripple [31] originates from the random orientation of the local magnetic anisotropy of individual crystallites [23–26]. Annealed sample 2 does not display visible Néel domain walls (Fig. 2d, e), but its ripple amplitude is noticeably higher than that of sample 1.

3.3. Microwave properties

Using the scanning FMR spectrometer, we determined the effective saturation magnetization M_{eff} and the field H_u of the uniaxial anisotropy induced by an external magnetic field during films sputtering. This was done by measuring the absorption spectra from local areas (1 mm^2) and with a step of 1 mm over the whole film surface. The measurement results for samples 1 and 2 are shown in Fig. 3. Relatively high uniformity in the distribution of magnetic

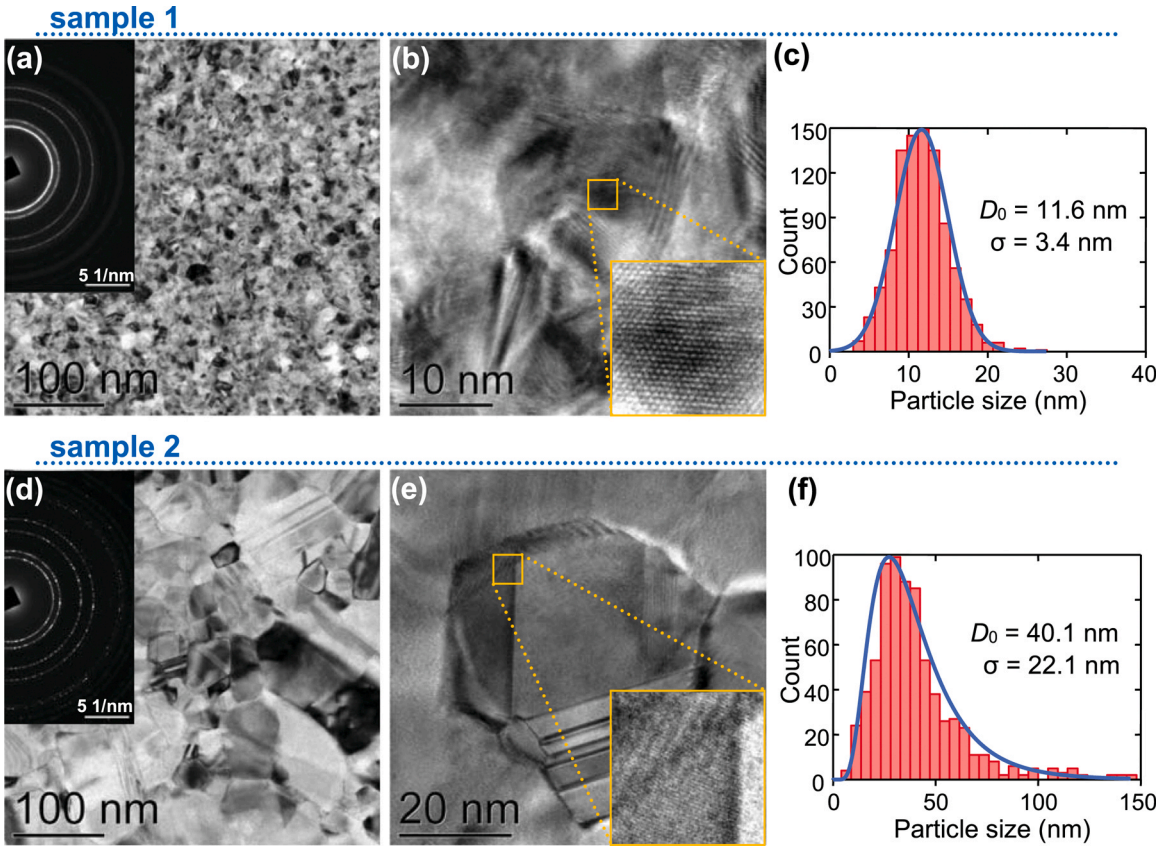

Fig. 1. a, d TEM images, b, e HRTEM images, and c, f crystallite size distributions for samples 1 and 2. Insets in a, d show SAED patterns for the corresponding samples.

parameters is observed in the central part of the films. However, as we approach films' edges, the uniaxial anisotropy field H_u substantially deviates, and the effective saturation magnetization M_{eff} noticeably decreases. It has been shown in Refs. [46,48] that these edge effects were caused by the nonuniform demagnetizing fields originated at the film edges.

The averaged values of the measured parameters for samples 1 and 2 are listed in Table 1. As it follows from the table, the annealing at 350 °C for 3 h resulted in the increase of the effective magnetization M_{eff} from 873.4 to 915 emu/cm^3, and the decrease of the anisotropy field H_u from 4 to 3.2 Oe. These changes in magnetic parameters are caused by the growth of the crystalline phase and the decrease of the relative fraction of the intergranular amorphous phase.

Using the VNA-FMR spectrometer, we investigated the microwave characteristics of the samples in a broad range of applied magnetic fields H and frequencies f. Fig. 4b and d show the imaginary part of the magnetic permeability $\mu = \mu' - i\mu''$ versus f and H for samples 1 and 2, when the static external magnetic field H was applied along the hard axis (HA) of magnetization. Note that the maximum of the microwave energy absorption, described by the imaginary part of permeability μ'', is observed when the frequency of the driving field $f = \omega/2\pi$ is equal to the FMR frequency of the film. In this case, $\mu''_{max} \approx \omega_M/\alpha\omega$, where $\omega_M = \gamma 4\pi M_s$, $\gamma = 1.76 \times 10^7$ rad/s Oe is the gyromagnetic ratio, and α is the dimensionless damping parameter. As the applied field H increases, the FMR frequency increases as well, resulting in the decrease of the μ''_{max} proportionally to ω. Therefore, to make the details of the FMR spectra clearly visible for

Table 1
Summary table of thin films parameters.

Parameters	sample 1	sample 2
Structure parameters[a]		
Average crystallite size D_0 (nm)	11.6	40.1
Standard deviation of crystallite size σ (nm)	3.4	22.1
Chemical composition[b]		
Fe/Ni (at%)	20/80	20/80
Magnetic parameters[c]		
Effective saturation magnetization M_{eff} (emu/cm^3)	873.4 ± 6.2	915.0 ± 7.6
In-plane uniaxial anisotropy field H_u (Oe)	4.0 ± 0.21	3.2 ± 0.26
In-plane uniaxial anisotropy constant $K_u = H_u M_{eff}/2$ (erg/cm^3)	$(1.75 \pm 0.07) \times 10^3$	$(1.46 \pm 0.11) \times 10^3$
Fitting parameters of the micromagnetic model		
Local uniaxial anisotropy constant K (erg/cm^3)	12.55×10^4	6.90×10^4
Exchange constant A (erg/cm)	1×10^{-6}	1×10^{-6}
Damping parameter α	0.0065	0.0065

[a] TEM analysis.
[b] EDS analysis.
[c] Scanning FMR spectrometer.

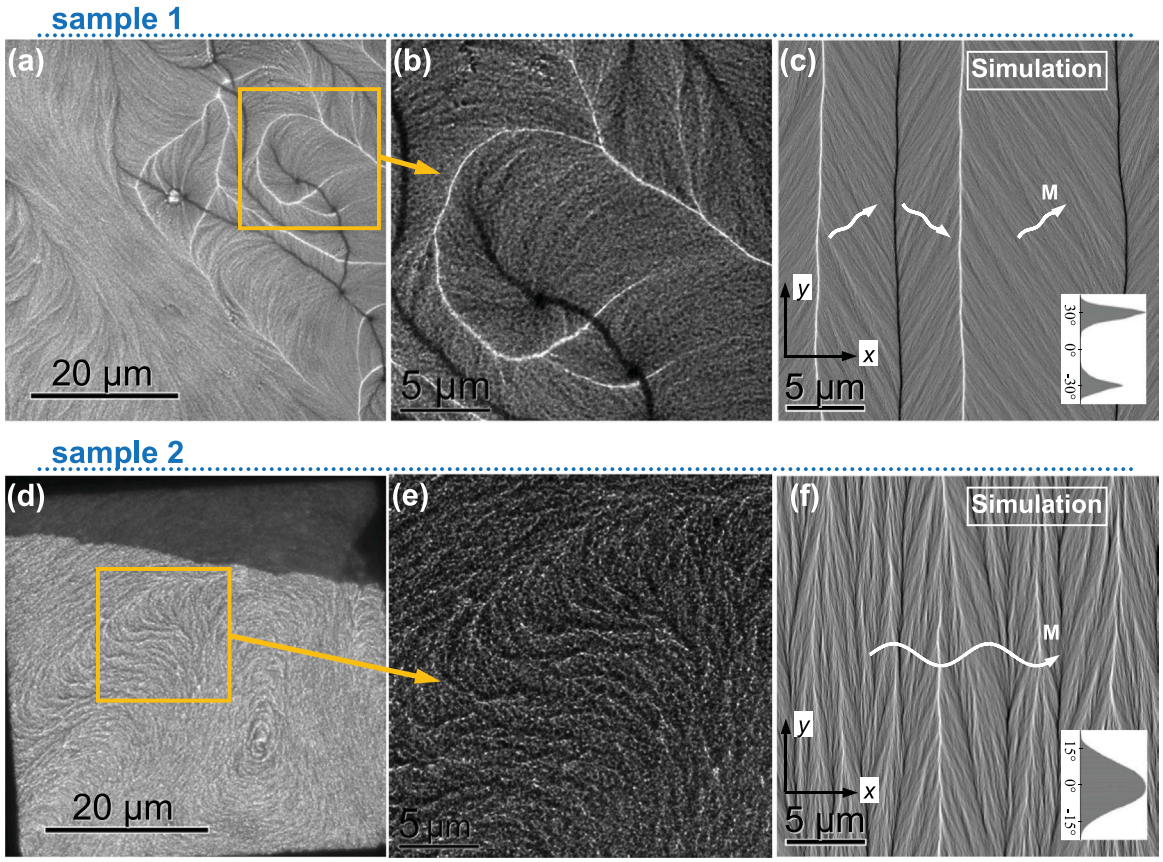

Fig. 2. Lorentz TEM images for samples 1 (a, b) and 2 (d, e), and magnetic structures obtained using micromagnetic simulations for samples 1 (c) and 2 (f). Insets in c and f show the distribution of the magnetic moments depending on the angle of their deviation from the *x*-axis.

all frequency range from 0 to 8 GHz, in Fig. 4b, d we show normalized dependencies $\mu''(f,H)\cdot\omega/\omega_M$. This normalization allowed us to represent $\mu''(f,H)$ spectra on the same scale and to enhance the visual perception of regions on the $\mu''(f,H)$-maps (Fig. 4b, d) with the maximum broadening of the FMR line. As an example, in Fig. 4a, c the solid lines show the fragments of the normalized FMR spectra $\mu'(H)$ and $\mu''(H)$ at a frequency of $f = 4$ GHz.

The phenomenological theory of ferromagnetic resonance for a single domain (SD) thin film with uniaxial magnetic anisotropy gives the following simple expression for the magnetic permeability [13].

$$\mu(f,H) = \mu' - i\mu'' = 1 + \frac{\omega_M\omega_z}{\omega_0^2 - \omega^2 + i\alpha\omega(\omega_z+\omega_y)}, \quad (2)$$

where $\omega_0 = 2\pi f_0 = \sqrt{\omega_z\omega_y}$ is the frequency of the uniform FMR mode. When the film is magnetized along the HA (as in the experiment), the values of ω_z and ω_y can be determined from the conditions

$$\begin{aligned} &\omega_z = \gamma(4\pi M_s + H_u); \quad \omega_y = \gamma(H_u^2 - H^2)/H_u \quad \text{for} H \le H_u, \\ &\omega_z = \gamma(4\pi M_s + H); \quad \omega_y = \gamma(H - H_u) \quad \text{for} H \ge H_u. \end{aligned} \quad (3)$$

The dashed lines in Fig. 4a, c show the theoretical dependencies $\mu'(H)$ and $\mu''(H)$ calculated using Eq. (2) for the experimental parameters of the films. Comparing the theoretical and experimental curves, one can see that the nanocrystalline structure of the films leads to the shift of the resonance field and broadening of the FMR line. This transformation of the FMR spectrum is more pronounced for sample 2, which average crystallite size 3.5 times larger than that of sample 1.

As was already mentioned in the introduction, the FMR linewidth of any magnetic material is primarily determined by its intrinsic damping parameter. However, inhomogeneities in magnetic samples become the source of another – extrinsic – relaxation mechanisms. Among them, the two-magnon scattering processes are of the most importance [13]. To separate the intrinsic and extrinsic contributions to the relaxation, it is convenient to express the measured resonance field H_R and FMR linewidth ΔH as sums consisting of two terms

$$\begin{aligned} H_R &= H_0 + H^{(2m)}, \\ \Delta H &= \Delta H_0 + \Delta H^{(2m)}, \end{aligned} \quad (4)$$

where the first term on the right side of each expression describes the uniform FMR of a thin film without considering its inhomogeneous structure, while the second one accounts for the two-magnon scattering of spin waves on inhomogeneities (this will be discussed later in Section 3.5). Here, the resonance field H_0 should satisfy the condition $\omega_0 = 2\pi f_0 = \sqrt{\omega_z\omega_y}$, and the FMR linewidth is determined by the well-known expression $\Delta H_0 = 4\pi f_0\alpha/\gamma$ [13]. With theoretical values for H_0 and ΔH_0, we can extract $H^{(2m)}$ and $\Delta H^{(2m)}$ from the measured H_R and ΔH using Eq. (4).

Fig. 5a, b shows the additional contributions to the FMR linewidth $\Delta H^{(2m)}$ and resonance field shift $H^{(2m)}$ as a function of the frequency f_0. These dependencies were obtained from the experimental data for sample 1 (triangle symbols) and sample 2 (circles). First of all, one can see significant broadening and shift of the resonance field occurring for both samples at low frequencies below 1 GHz. This can be easily understood from Fig. 4b and d, where insets show normalized dependencies $\mu''(H)$ at a frequency of 0.6 GHz (sample 1) and 0.8 GHz (sample 2). An additional peak can be seen in the FMR spectrum for the field $H \approx H_u$ when the film was magnetized along the HA. This peak, which was first revealed in the work [49], leads to the distortion of the spectrum, and, consequently, to the FMR line broadening and resonance field shift. At higher frequencies (above 1 GHz), the dependence $\Delta H^{(2m)}$ of sample 1 monotonically

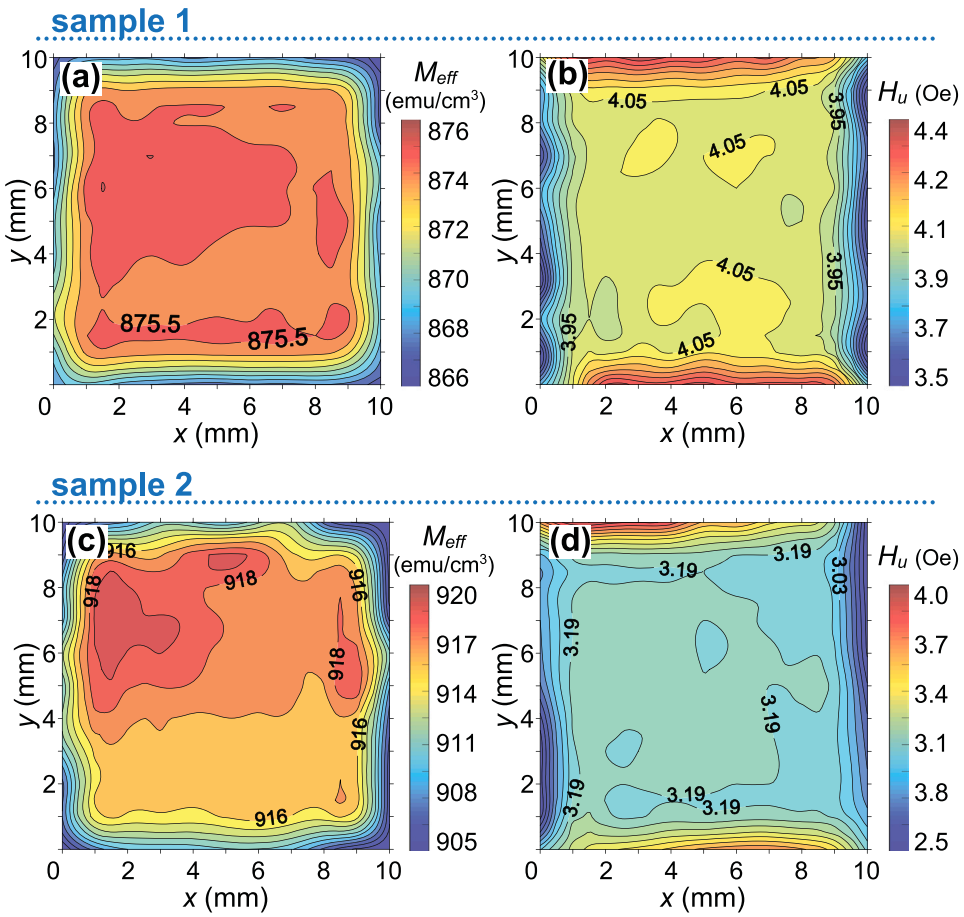

Fig. 3. Distribution of the effective saturation magnetization M_{eff} and uniaxial anisotropy field H_u over the surface of the sample 1 (a, b) and sample 2 (c, d).

increases with f_0. This behavior agrees well with the two-magnon scattering theory developed by Arias and Mills for the inhomogeneous ultrathin films [17]. However, sample 2 exhibits substantial broadening of the FMR line with the maximum value of $\Delta H^{(2m)} \approx 14$ Oe at a frequency of $f_0 \approx 5$ GHz.

The broadening of the FMR line is also accompanied by the shift of the resonance field on the value $H^{(2m)}$ relative to the field H_0. As Fig. 5b demonstrates, the dependence $H^{(2m)}(f_0)$ of sample 1 first gradually increases with the increase of the resonance frequency f_0, achieving the maximum of 1.8 Oe at $f_0 \approx 5$ GHz, and then decreases monotonically down to 1 Oe. Similar but more distinct behavior of $H^{(2m)}(f_0)$ is observed for sample 2. The shift of the resonance field is reaching its maximum of 4.5 Oe at a frequency of $f_0 \approx 4.5$ GHz and becomes close to zero at $f_0 \approx 9.5$ GHz.

3.4. Results of micromagnetic simulation

To study the FMR line broadening and shift effect, we performed micromagnetic simulations of the magnetic microstructure and microwave permeability of the films. The parameters used in micromagnetic simulations for samples 1 and 2 are listed in Table 1. Note that in the simulation, we applied experimental values for the saturation magnetization $M_s = M_{eff}$ and induced uniaxial anisotropy constant K_u. For both samples, the same value of damping parameter α accounting for intrinsic relaxation was used. The value of $\alpha = 0.0065$ was estimated from the experimental data for sample 1 recorded at a frequency of $f_0 \approx 9.5$ GHz. A typical for permalloy ($Fe_{20}Ni_{80}$) value of the exchange constant $A = 1 \times 10^{-6}$ erg/cm was used.

An important parameter of the numerical model is the local magnetic anisotropy constant K. Apart from the magnetocrystalline anisotropy of individual crystallites, other sources of the local anisotropy can be local stresses [22,50] and their gradients [51] arising from the thermal expansion coefficient mismatch between film and substrate, or lattice defects. Also, surface magnetic anisotropy plays an important role in nanosized particles. It was empirically found [52] that the contribution of the surface anisotropy to the effective local magnetic anisotropy increases with the decrease of crystallite size as $K = K_v + 6K_s/D_0$, where K_v and K_s are the volume and surface anisotropy constants. In this work, the value of K was fitted to achieve the best agreement between numerical and experimental results. It has turned out that K of sample 1 was 1.8 times larger than K of sample 2 (see Table 1). In our opinion, this is due to the influence of the surface anisotropy of crystallites. The estimate of the volume and surface anisotropy constants for these values of K yields the reasonable values $K_v = 4.6 \times 10^4$ erg/cm^3, and $K_s = 1.54 \times 10^{-2}$ erg/cm^2.

Numerical simulations of the magnetic microstructure of the nanocrystalline films were performed for the case when an external magnetic field H was applied along the hard axis. In a Cartesian coordinate system, which xy plane coincided with the film plane, the direction of the HA was chosen to lie along the x-axis. First, the film was saturated with a magnetic field of 100 kOe, and then the field was decreased to zero with a constant (on a logarithmic scale) step dH ($\lg dH = 0.1$). For sample 1, the decrease of the field H first led to the rise of the fluctuations (ripple) of the magnetization **M**, and then to the incoherent rotation of the magnetization at separate regions toward the y-axis and formation of low-angle domain walls oriented orthogonally to the field and HA. Fig. 2c presents the $\partial M_y/\partial x$

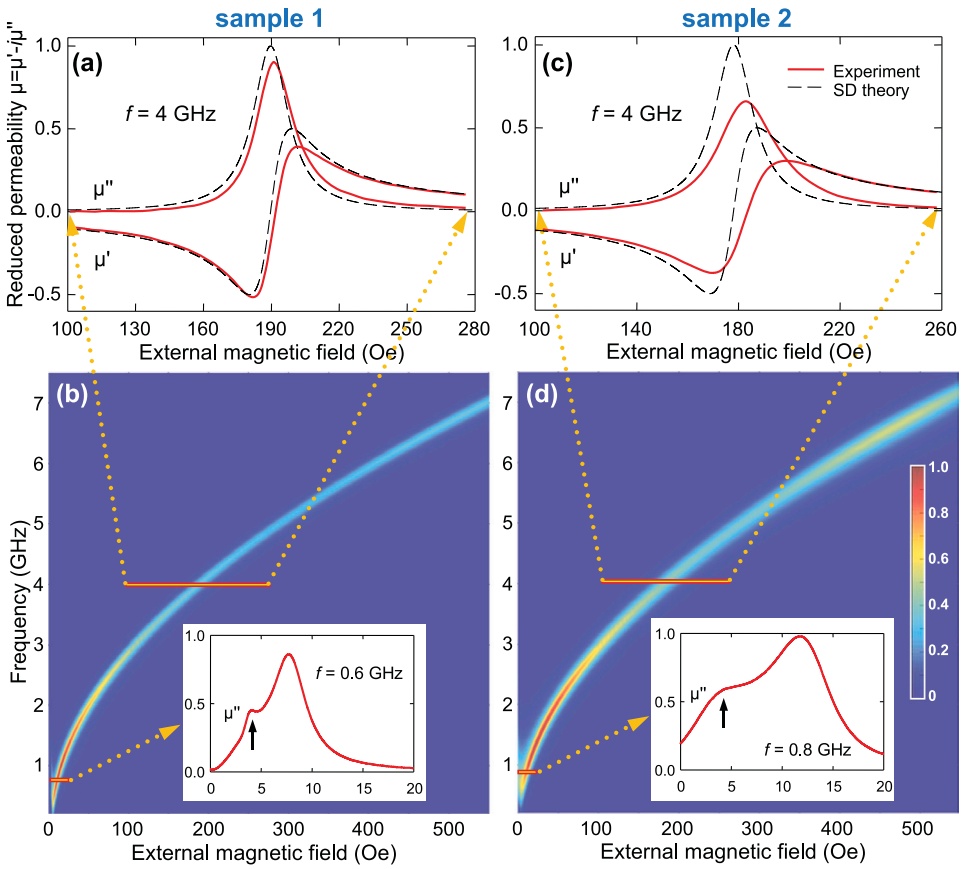

Fig. 4. Results of VNA-FMR measurements. a, c Normalized real μ' and imaginary μ'' parts of the magnetic permeability as a function of an external magnetic field H measured at a frequency of $f = 4$ GHz (solid lines), and calculated using Eq. (2) (dashed lines) for samples 1 and 2. b, d Normalized dependencies $\mu''(f,H)\cdot\omega/\omega_M$ for samples 1 and 2. Insets in b, d show fragments of normalized spectra $\mu''(H)$ measured at the indicated frequencies.

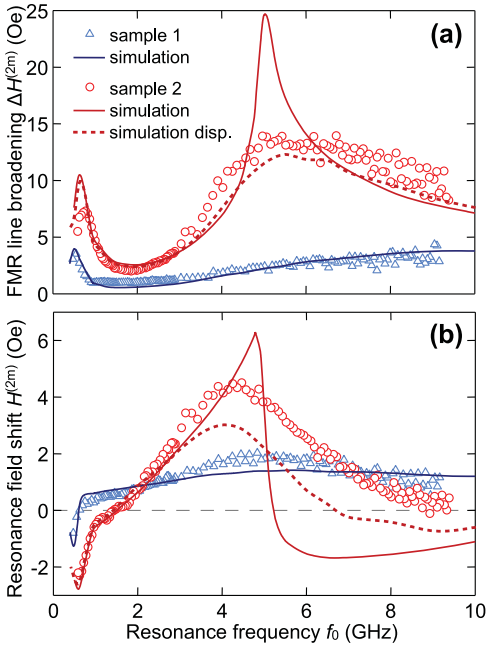

Fig. 5. Frequency dependencies of FMR line broadening $\Delta H^{(2\,m)}$ (a) and resonance field shift $H^{(2\,m)}$ (b) obtained experimentally with VNA-FMR (symbols) and from micromagnetic simulations (lines) for samples 1 and 2.

distribution calculated for $H = 0$, showing qualitative agreement with Lorentz TEM images in Fig. 2b. The arrows in Fig. 2c schematically depict the direction of the magnetization **M** in magnetic domains, while the inset shows the statistical distribution of the crystallites' magnetic moments depending on the angle of their deviation from the average magnetization. For sample 2, the field decrease also resulted in the magnetization fluctuations (ripple) increase, but for the field of $H = 0$ (Fig. 2f), there is no defined domain structure.

With the micromagnetic simulation of the microwave permeability of the films, we studied the features of FMR line broadening $\Delta H^{(2m)}$ and resonance field shift $H^{(2m)}$. The solid lines in Fig. 5a and b show numerically calculated dependencies $\Delta H^{(2m)}(f_0)$ and $H^{(2m)}(f_0)$. For sample 1, simulation results are in good quantitative agreement with the experimental data. A slight discrepancy might be related to the dispersion of the crystallite size in the real sample (see Fig. 1c), as in the numerical model all crystallites had the same size D_0.

The simulation for sample 2 shows that the frequency dependence of the FMR line broadening $\Delta H^{(2m)}$ has a sharp peak at a frequency of ~ 5 GHz (Fig. 5a). This sharp increase in the FMR line broadening is also accompanied by a substantial shift of the resonance field $H^{(2m)}$ both to the positive and negative values. Furthermore, $H^{(2m)}$ changes sign near the frequency position of the FMR line broadening maximum (Fig. 5b). As can be seen, the simulations are in reasonable agreement with the experimental results. Although the large crystallite size dispersion of sample 2 (Fig. 1f) apparently results in smoothing of the sharp peak visible on numerically calculated $\Delta H^{(2m)}(f_0)$ and also smoothing of $H^{(2m)}(f_0)$ curve.

To verify this suggestion, we calculated absorption spectra for 15 nanocrystalline films that differed only in crystallite size, ranging from 10.1 to 80.1 nm with 5 nm step. Other magnetic parameters were the same and corresponded to the parameters used in micromagnetic simulations of sample 2. We then calculated the weighted

sum of the obtained spectra according to the function of crystallite size distributions for sample 2 (Fig. 1f). The broadening and shift of the obtained "integral" FMR lines are shown by dashed lines in Fig. 5. One can see that the dispersion in crystallite sizes indeed results in the smoothing of $\Delta H^{(2m)}(f_0)$ and $H^{(2m)}(f_0)$ dependencies obtained by simulation for sample 2 with D_0 = 40.1 nm. Overall, a better agreement between the results of numerical calculations and the experiment is achieved. The lack of complete matching is probably because of the necessity of considering in the model not only the crystallite size dispersion but also the dispersion of the saturation magnetization and the local magnetic anisotropy constant, which are almost invariably present in nanocrystalline materials.

3.5. Mechanism of the FMR line broadening

In this section, we will address the revealed for sample 2 effect of the sharp FMR line broadening at a frequency of ~ 5 GHz and answer the question of why it is not observed for sample 1. First, we will consider the influence of the nanocrystalline structure of a thin film on the formation of its magnetic structure. Then we will reveal the role that magnetic structure plays in the two-magnon scattering and determine the critical crystallite size below which the effect of sharp FMR line broadening disappears.

3.5.1. Relation between crystalline and micromagnetic structures

Fig. 6 presents the general scheme of the magnetic structure formation in nanocrystalline thin magnetic films. The main feature of such films is their small crystallite size D_0 in comparison with the effective radius of the exchange and dipolar interactions. The magnetic coupling between crystallites averages and partially suppresses the local magnetic anisotropy in randomly oriented crystallites. But in most cases, the random anisotropy is not suppressed completely, and the magnetization vector **M** in different areas of the film deviates slightly from its mean direction. As a result, a unique quasi-periodic magnetic structure with spatial magnetization oscillations around some average direction is formed in the nanocrystalline thin film. This structure, as noted earlier, is called magnetization ripple [23–26].

The static theory of such fine magnetic structure was considered in the most detail in the works of Hoffmann [23,24]. Hoffmann, based on the results of Lorentz TEM, developed a model of non-interacting "particles" – magnetically coupled regions formed in the film (see Fig. 6). The shape of such "particles" is generally an ellipsoid, strongly elongated in the direction orthogonal to the external field. And their size is determined by the strength of the external magnetic field, as well as the radius of the exchange and dipolar interactions. When the film is magnetized along the HA, the length of the ellipsoid semiaxis $R_{||}$ in the linear approximation [23] is

$$R_{||} = \sqrt{D/(H - H_u)}, \quad (5)$$

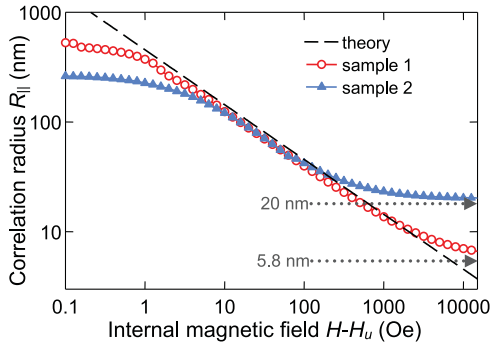

Fig. 7. Longitudinal correlation radius $R_{||}$ versus effective internal magnetic field for samples 1 (circles) and 2 (triangles). The dashed line shows the theoretical dependence calculated with Eq. (5).

where $D = 2A/M_s$. By averaging the random magnetic anisotropy within the magnetically coupled region, Hoffmann derived an expression for the magnetization dispersion, and the most probable dominant wavelength of the ripple in the longitudinal direction, $\lambda_R = 2\pi R_{||} = 2\pi\sqrt{D/(H - H_u)}$. Using a correlation analysis method [30] on the magnetic structures obtained with micromagnetic simulations for samples 1 and 2, we estimated the spatial length of magnetic correlations, that is, we determined an average size of the magnetically coupled region $R_{||}$along the direction of an average magnetization. The calculated for samples 1 and 2 dependencies of $R_{||}$ on an effective internal magnetic field $H - H_u$ are plotted in Fig. 7. The dashed line in this figure shows the theoretical dependence calculated with Eq. (5) for the parameters of sample 1, and it is almost the same for sample 2 (not shown).

The linear theory of Hoffmann is in good agreement with the simulation results for magnetic fields ranging from 1 to 1000 Oe for sample 1, and from 10 to 100 Oe for sample 2. At the large strength of the internal field $H - H_u$, the size of the magnetically coupled region is limited by the crystallite size. As Fig. 7 shows, the longitudinal correlation radius $R_{||}$ tends to R=$D_0/2$ for $H - H_u \to \infty$. In weak fields, the results of the numerical simulation and theory are also in disagreement. This discrepancy emerges because in weak fields the magnitude of magnetization ripple significantly increases, and the linear approximation used by Hoffmann for deriving Eq. (5) becomes invalid [23,25].

3.5.2. Two-magnon model of FMR damping

The quasiperiodic magnetization fluctuations with wavelength λ_R are the source of the magnetic inhomogeneities in the nanocrystalline thin magnetic films, with the characteristic size $R_{||}$ and wavenumber $k_R = 2\pi/\lambda_R = 1/R_{||}$. Note that, according to Eq. (5), the size of these inhomogeneities depends not only on the magnetic parameters of the film, but also on the strength of the effective internal

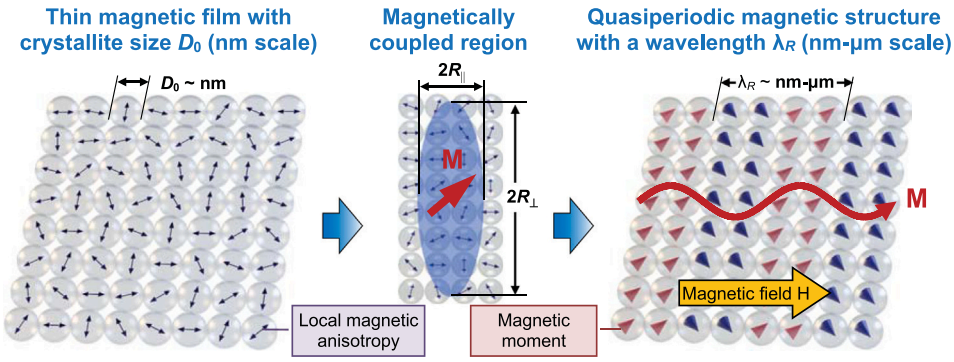

Fig. 6. Schematic illustration of the quasiperiodic magnetic structure formation in a nanocrystalline thin magnetic film.

field. In the two-magnon scattering theory [13,15,17], magnetic inhomogeneities (particularly originated from the nonuniform magnetic structure) are treated as a perturbation of the eigenmodes (spin waves) of the uniform film. Inhomogeneities disturb the orthogonality of the eigenmodes and lead to their interaction. Thus, the energy of the considered type of oscillations (particularly the uniform FMR mode) can leak into the other modes, providing an additional channel of dissipation.

Let us consider in more detail the mechanism of two-magnon scattering in thin magnetic films. The dispersion equation for spin waves, in the case of the uniaxial thin film uniformly magnetized along the HA, has the following form [17].

$$\omega_k = \gamma\sqrt{[H + Dk^2 + 4\pi M_s N_k][H - H_u + Dk^2 + 4\pi M_s \sin^2\phi_k(1 - N_k)]}. \quad (6)$$

Here φ_k is the angle between the mean magnetization and the propagation direction of a spin wave with wavenumber k, and N_k is the demagnetization factor. According to [25], this factor for a thin film can be expressed as

$$N_k(k, d) = \frac{1 - e^{-kd}}{kd}. \quad (7)$$

It has been shown in Ref. [17] that the scattering of spin waves on inhomogeneities only possible if $\varphi_k \approx 0$. The dispersion Eq. (6) for this case is shown in Fig. 8a, where ω_0 is the frequency of the uniform FMR (spin wave with $k = 0$). As can be seen from the figure, the uniform mode frequency coincides with the frequency of a spin wave with $k = k_s$. For the effective transfer of the uniform mode energy to the energy of the spin wave with wavenumber k_s a nonuniform periodic magnetic field with the wavenumber $k_R = k_s$ is required. This is the process of two-magnon scattering of spin waves on inhomogeneities, which results in the FMR line broadening and resonance field shift.

Using the following equation

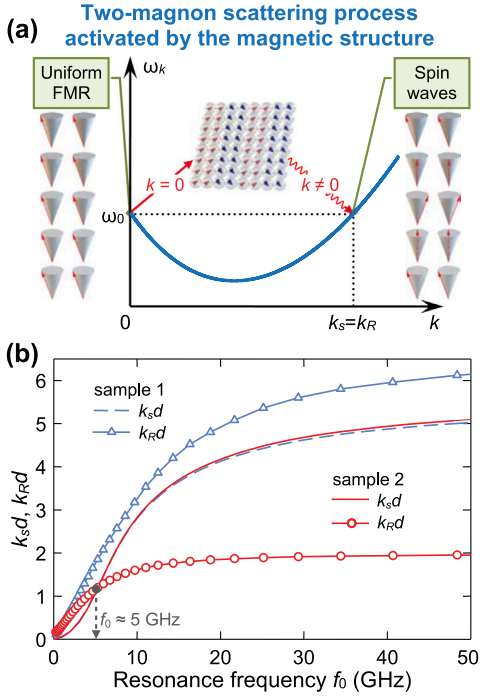

Fig. 8. a Spin-wave dispersion Eq. (6) and illustration of the two-magnon scattering on the quasiperiodic magnetic structure – magnetization ripple. b Frequency dependencies of the maximum wavenumber k_s calculated with Eq. (8) and the magnetization ripple wavenumber k_R obtained by micromagnetic simulations for samples 1 and 2.

$$\omega_k(H_0, k_s, \phi_k = 0) = \omega_0 \quad (8)$$

for the parameters of samples 1 and 2, we calculated the dependencies of k_s on the resonance frequency $f_0 = \omega_0/2\pi$. These dependences are shown in Fig. 8b by dashed and solid lines in the range of up to 50 GHz. Also, in this figure we plotted dependencies $k_R(f_0) = 1/R_{||}(f_0)$ for both samples, using the longitudinal correlation radius values obtained by the micromagnetic simulation (Fig. 7). The data plotted in Fig. 8b help explain why there is no sharp FMR line broadening for sample 1 with the average crystallite size of $D_0 = 11.6$ nm – the dependence $k_R(f_0)$ does not cross the $k_s(f_0)$ curve, meaning that the condition $k_s = k_R$ at which the effect emerges cannot be met in all frequency range. Contrary to that, the dependencies $k_R(f_0)$ and $k_s(f_0)$ calculated for sample 2 with the average crystallite size $D_0 = 40.1$ nm intersect at a point of $f_0 \approx 5$ GHz. And for this frequency, the maximum scattering of spin waves (in our case, uniform mode) on the magnetic inhomogeneities of the magnetization ripple is indeed observed.

In our previous work [30], we derived an expression for estimating the critical crystallite size D_{cr}, above which the effect of the sharp FMR line broadening occurs. This expression is easy to obtain if we take into account that with an increase in the resonance frequency f_0 (or resonance field H_0), the wavenumber k_R of the magnetization ripple tends to the limit $k_R(\infty) = 2/D_0$ (see Section 3.5.1), and the wavenumber k_s grows monotonically until a certain saturation value $k_s(\infty)$. From Eqs. (7) and (8), we have

$$k_s(\infty) = \sqrt{2\pi(1 - N_k(k_s, d))}/L_{ex}, \quad (9)$$

where a characteristic parameter – the exchange length $L_{ex} = \sqrt{2A/M_s^2}$ is determined by the competition between the exchange and dipolar energies [11]. As can be seen directly from Fig. 8b, the criterion $k_R(\infty) = k_s(\infty)$ allows one to obtain the expression for the estimating of critical crystallite size D_{cr} as

$$D_{cr} = g(d/D_{cr})\cdot L_{ex}. \quad (10)$$

The function $g(d/D_{cr}) = \sqrt{2/\pi(1 - N_k(k = 2/D_{cr}, d))}$ in (10) rapidly decreases with the increase of the ratio of the film thickness to the crystallite size d/D_{cr} and tends to the constant value of about 0.8. Therefore, for sufficiently thick films compared to the crystallite size ($d/D_{cr} > 5$), the critical size approximately equals $D_{cr} \approx 0.8\, L_{ex}$. When the crystallite size is comparable to the nanocrystalline film thickness, the critical size is $D_{cr} \approx L_{ex}$. The calculation of D_{cr} with Eq. (10) for the parameters of the experimental samples gives a value of 14.3 nm, which agrees with the experimental results shown in Fig. 5.

4. Conclusions

In this paper we have experimentally revealed and explored theoretically a new effect of sharp broadening and shift of the ferromagnetic resonance line in nanocrystalline thin magnetic films. The studies were carried out on samples of nanocrystalline permalloy ($Fe_{20}Ni_{80}$) films 40 nm in thickness with different crystallite sizes. Based on the results of structural and magneto-structural studies, as well as the results of micromagnetic simulations, we have demonstrated that this effect is caused by the scattering of spin waves on the quasiperiodic magnetic structure of magnetization ripple that emerges in nanocrystalline films due to the random orientation of the crystallite magnetic anisotropy. The revealed effect is of the threshold nature as it can only occur when the crystallite size of a film is greater than the critical value D_{cr}. Generally, the critical crystallite size D_{cr} depends on the thickness, the exchange constant A, and the saturation magnetization M_s of the film, but it can be approximated as $D_{cr} \approx L_{ex}$, where the characteristic parameter $L_{ex} = \sqrt{2A/M_s^2}$ is determined by the competition between the exchange and dipolar energies. This work extends our understanding of the relationship between nanostructure–magnetic

structure–magnetization dynamics and opens up new possibilities for optimizing microwave characteristics of nanocrystalline thin films.

CRediT authorship contribution statement

A.V. Izotov: Conceptualization, Methodology, Software, Writing – original draft, Supervision. **B.A. Belyaev:** Conceptualization, Supervision, Writing – review & editing, Funding acquisition. **N.M. Boev:** Software, Visualization. **A.V. Burmitskikh:** Investigation, Methodology. **G.V. Skomorokhov:** Investigation, Visualization. **S.M. Zharkov:** Investigation, Methodology, Writing – original draft. **P.N. Solovev:** Conceptualization, Methodology, Writing – original draft.

Declaration of Competing Interest

The authors declare that they have no known competing financial interests or personal relationships that could have appeared to influence the work reported in this paper.

Acknowledgments

The reported study was funded by RFBR, the Government of Krasnoyarsk Territory, Krasnoyarsk Regional Fund and JSC "NPP "Radiosviaz", project number 20-42-242901 and was supported by the Ministry of Science and Higher Education of the Russian Federation, agreement number 075-11-2019-054 dated 22.11.2019.

The electron microscopy investigations were conducted in the SFU Joint Scientific Center whose infrastructure was supported by the State assignment (#FSRZ-2020-0011) of the Ministry of Science and Higher Education of the Russian Federation.

References

[1] V.G. Harris, Microwave magnetic materials, in: K.H.J. Buschow (Ed.), Handbook of Magnetic Materials, Imprint, University of Amsterdam, Elsevier B.V., Northholland, 2012, pp. 1–63, https://doi.org/10.1016/B978-0-444-56371-2.00001-5

[2] Y. Yoshizawa, S. Oguma, K. Yamauchi, New Fe-based soft magnetic alloys composed of ultrafine grain structure, J. Appl. Phys. 64 (1988) 6044–6046, https://doi.org/10.1063/1.342149

[3] H. Lee, K.-J. Lee, Y.-K. Kim, K. Kim, S.-C. Yu, Ultra-soft magnetic properties in nanocrystalline Fe81B11Nb7Cu1 alloy, J. Alloy. Compd. 326 (2001) 313–316, https://doi.org/10.1016/S0925-8388(01)01291-9

[4] K. Suzuki, N. Kataoka, A. Inoue, A. Makino, T. Masumoto, High saturation magnetization and soft magnetic properties of bcc Fe-Zr-B alloys with ultrafine grain structure, Mater. Trans. JIM 31 (1990) 743–746, https://doi.org/10.2320/matertrans1989.31.743

[5] M.A. Willard, D.E. Laughlin, M.E. McHenry, D. Thoma, K. Sickafus, J.O. Cross, V.G. Harris, Structure and magnetic properties of (Fe0.5Co0.5)88Zr7B4Cu1 nanocrystalline alloys, J. Appl. Phys. 84 (1998) 6773–6777, https://doi.org/10.1063/1.369007

[6] H.L. Seet, X.P. Li, Z.J. Zhao, Y.K. Kong, H.H. Zheng, W.C. Ng, Development of high permeability nanocrystalline permalloy by electrodeposition, J. Appl. Phys. 97 (2005) 10N304, https://doi.org/10.1063/1.1855712

[7] I. Fergen, K. Seemann, A. v.d. Weth, A. Schüppen, Soft ferromagnetic thin films for high frequency applications, J. Magn. Magn. Mater. 242–245 (2002) 146–151, https://doi.org/10.1016/S0304-8853(01)01185-4

[8] C.V. Falub, R. Hida, M. Meduna, J. Zweck, J.-P. Michel, H. Sibuet, D. Schneider, M. Bless, J.H. Richter, H. Rohrmann, Structural and ferromagnetic properties of sputtered FeCoB/AlN soft magnetic multilayers for GHz applications, IEEE Trans. Magn. 53 (2017) 1–6, https://doi.org/10.1109/TMAG.2017.2703175

[9] A.N. Lagarkov, K.N. Rozanov, High-frequency behavior of magnetic composites, J. Magn. Magn. Mater. 321 (2009) 2082–2092, https://doi.org/10.1016/j.jmmm.2008.08.099

[10] O. Acher, A.L. Adenot, Bounds on the dynamic properties of magnetic materials, Phys. Rev. B 62 (2000) 11324–11327, https://doi.org/10.1103/PhysRevB.62.11324

[11] S. Shukla, P.K. Deheri, R.V. Ramanujan, Magnetic nanostructures: synthesis, properties, and applications, in: R. Vajtai (Ed.), Springer Handbook of Nanomaterials, Springer, Berlin Heidelberg, Berlin, Heidelberg, 2013, pp. 473–514, https://doi.org/10.1007/978-3-642-20595-8_12

[12] A. Barman, J. Sinha, Spin Dynamics and Damping in Ferromagnetic Thin Films and Nanostructures, Springer International Publishing, Cham, 2018 ISBN 978-3-319-66296-1.

[13] A.G. Gurevich, G.A. Melkov, Magnetization Oscillations and Waves, CRC Press, Boca Raton, 1996 ISBN 978-0849394607.

[14] R.D. McMichael, D.J. Twisselmann, A. Kunz, Localized ferromagnetic resonance in inhomogeneous thin Films, Phys. Rev. Lett. 90 (2003) 227601, https://doi.org/10.1103/PhysRevLett.90.227601

[15] R.D. McMichael, P. Krivosik, Classical model of extrinsic ferromagnetic resonance linewidth in ultrathin films, IEEE Trans. Magn. 40 (2004) 2–11, https://doi.org/10.1109/TMAG.2003.821564

[16] S.S. Kalarickal, P. Krivosik, J. Das, K.S. Kim, C.E. Patton, Microwave damping in polycrystalline Fe-Ti-N films: physical mechanisms and correlations with composition and structure, Phys. Rev. B 77 (2008) 054427, https://doi.org/10.1103/PhysRevB.77.054427

[17] R. Arias, D.L. Mills, Extrinsic contributions to the ferromagnetic resonance response of ultrathin films, Phys. Rev. B 60 (1999) 7395–7409, https://doi.org/10.1103/PhysRevB.60.7395

[18] G. Woltersdorf, B. Heinrich, Two-magnon scattering in a self-assembled nanoscale network of misfit dislocations, Phys. Rev. B 69 (2004) 184417, https://doi.org/10.1103/PhysRevB.69.184417

[19] I. Barsukov, F.M. Romer, R. Meckenstock, K. Lenz, J. Lindner, S. Hemken to Krax, A. Banholzer, M. Korner, J. Grebing, J. Fassbender, M. Farle, Frequency dependence of spin relaxation in periodic systems, Phys. Rev. B 84 (2011) 140410, https://doi.org/10.1103/PhysRevB.84.140410

[20] L. Lu, J. Young, M. Wu, C. Mathieu, M. Hadley, P. Krivosik, N. Mo, Tuning of magnetization relaxa-tion in ferromagnetic thin films through seed layers, Appl. Phys. Lett. 100 (2012) 022403, https://doi.org/10.1063/1.3675614

[21] G. Herzer, Nanocrystalline soft magnetic materials, J. Magn. Magn. Mater. 157 (158) (1996) 133–136, https://doi.org/10.1016/0304-8853(95)01126-9

[22] G. Herzer, Modern soft magnets: amorphous and nanocrystalline materials, Acta Mater. 61 (2013) 718–734, https://doi.org/10.1016/j.actamat.2012.10.040

[23] H. Hoffmann, Theory of magnetization ripple, IEEE Trans. Magn. 4 (1968) 32–38, https://doi.org/10.1109/TMAG.1968.1066186

[24] H. Hoffmann, Quantitative calculation of the magnetic ripple of uniaxial thin permalloy films, J. Appl. Phys. 35 (1964) 1790–1798, https://doi.org/10.1063/1.1713743

[25] K.J. Harte, Theory of magnetization ripple in ferromagnetic films, J. Appl. Phys. 39 (1968) 1503–1524, https://doi.org/10.1063/1.1656388

[26] V.A. Ignatchenko, Magnetic structure of thin magnetic films and ferromagnetic resonance, Sov. Phys. JETP 27 (1) (1968) 162–166 ⟨http://www.jetp.ac.ru/cgi-bin/dn/e_027_01_0162.pdf⟩.

[27] N.G. Chechenin, C.B. Craus, A.R. Chezan, T. Vystavel, D.O. Boerma, J.T.M. De Hosson, L. Niesen, Relation between observed micromagnetic ripple and FMR width in ultrasoft magnetic films, IEEE Trans. Magn. 38 (2002) 3027–3029, https://doi.org/10.1109/TMAG.2002.802123

[28] N.G. Chechenin, Micromagnetism and high-frequency properties of soft magnetic films, J. Magn. Magn. Mater. 300 (2006) 198–201, https://doi.org/10.1016/j.jmmm.2005.10.062

[29] V.A. Ignatchenko, G.V. Degtyarev, Resonant shift and broadening of FMR lines, due to fine magnetic structure, Sov. Phys. JETP 33 (2) (1971) 393–397 ⟨http://www.jetp.ac.ru/cgi-bin/dn/e_033_02_0393.pdf⟩.

[30] A.V. Izotov, B.A. Belyaev, P.N. Solovev, N.M. Boev, Grain-size dependence of magnetic microstructure and high-frequency susceptibility of nanocrystalline thin films: a micromagnetic simulation study, J. Magn. Magn. Magn. 529 (2021) 167856, https://doi.org/10.1016/j.jmmm.2021.167856

[31] H.W. Fuller, M.E. Hale, Determination of magnetization distribution in thin films using electron microscopy, J. Appl. Phys. 31 (1960) 238–248, https://doi.org/10.1063/1.1735552

[32] D.T. Ngo, L.T. Kuhn, In situ transmission electron microscopy for magnetic nanostructures, Adv. Nat. Sci. Nanosci. Nanotechnol. 7 (2016) 45001, https://doi.org/10.1088/2043-6262/7/4/045001

[33] J. Wei, J. Wang, Q. Liu, X. Li, D. Cao, X. Sun, An induction method to calculate the complex permeability of soft magnetic films without a reference sample, Rev. Sci. Instrum. 85 (5) (2014) 054705, https://doi.org/10.1063/1.4876598

[34] D. Pain, M. Ledieu, O. Acher, A.L. Adenot, F. Duverger, An improved permeameter for thin film measurements up to 6 GHz, J. Appl. Phys. 85 (1999) 5151–5153, https://doi.org/10.1063/1.369107

[35] B.A. Belyaev, A.V. Izotov, A.A. Leksikov, Magnetic imaging in thin magnetic films by local spectrometer of ferromagnetic resonance, IEEE Sens. J. 5 (2005) 260–266, https://doi.org/10.1109/JSEN.2004.842293

[36] B.A. Belyaev, N.M. Boev, A.A. Gorchakovsky, R.G. Galeev, Inspection probes of a ferromagnetic resonance scanning spectrometer, Instrum. Exp. Tech. 64 (2021) 277–284, https://doi.org/10.1134/S0020441221010218

[37] A. Belyaev, A.V. Izotov, P.N. Solovev, Competing magnetic anisotropies in obliquely deposited thin permalloyfilm, Physica B 481 (2016) 86–90, https://doi.org/10.1016/j.physb.2015.10.036

[38] B.A. Belyaev, A.V. Izotov, P.N. Solovev, I.A. Yakovlev, Determination of magnetic anisotropies and miscut angles in epitaxial thin films on vicinal (111) substrate by the ferromagnetic resonance, J. Magn. Magn. Mater. 440 (2017) 181–184, https://doi.org/10.1016/j.jmmm.2016.12.081

[39] P.N. Solovev, A.V. Izotov, B.A. Belyaev, Microstructural and magnetic properties of thin obliquely deposited films: a simulation approach, J. Magn. Magn. Mater. 429 (2017) 45–51, https://doi.org/10.1016/j.jmmm.2017.01.012

[40] J. Dubowik, Shape anisotropy of magnetic heterostructures, Phys. Rev. B 54 (1996) 1088–1091, https://doi.org/10.1103/PhysRevB.54.1088

[41] M.O. Liedke, M. Körner, K. Lenz, M. Fritzsche, M. Ranjan, A. Keller, E. Čižmár, S.A. Zvyagin, S. Facsko, K. Potzger, J. Lindner, J. Fassbender, Crossover in the

surface anisotropy contributions of ferromagnetic films on rippled Si surfaces, Phys. Rev. B 87 (2013) 024424, https://doi.org/10.1103/PhysRevB.87.024424
[42] B.A. Belyaev, A.V. Izotov, An.A. Leksikov, Micromagnetic calculation of the equilibrium distribution of magnetic moments in thin films, Phys. Solid State 52 (2010) 1664–1672, https://doi.org/10.1134/S1063783410080160
[43] A.V. Izotov, B.A. Belyaev, P.N. Solovev, N.M. Boev, Numerical calculation of high frequency magnetic susceptibility in thin nanocrystalline magnetic films, Physica B 556 (2019) 42–47, https://doi.org/10.1016/j.physb.2018.12.006
[44] A.J. Newell, W. Williams, D.J. Dunlop, A generalization of the demagnetizing tensor for nonuniform magnetization, J. Geophys. Res. 98 (1993) 9551, https://doi.org/10.1029/93JB00694
[45] K.M. Lebecki, M.J. Donahue, M.W. Gutowski, Periodic boundary conditions for demagnetization interactions in micromagnetic simulations, J. Phys. D Appl. Phys. 41 (2008) 175005, https://doi.org/10.1088/0022-3727/41/17/175005
[46] B.A. Belyaev, A.V. Izotov, G.V. Skomorokhov, P.N. Solovev, Experimental study of the magnetic characteristics of nanocrystalline thin films: the role of edge effects, Mater. Res. Express 6 (2019) 116105, https://doi.org/10.1088/2053-1591/ab4456
[47] F.N. Rhines, B.R. Patterson, Effect of the degree of prior cold work on the grain volume distribution and the rate of grain growth of recrystallized aluminum, Metall. Trans. A 13 (1982) 985–993, https://doi.org/10.1007/BF02643395
[48] B.A. Belyaev, A.V. Izotov, G.V. Skomorokhov, P.N. Solovev, Micromagnetic analysis of edge effects in a thin magnetic film during local excitation of magnetization oscillations, Russ. Phys. J. 63 (2020) 837–843, https://doi.org/10.1007/s11182-020-02106-3
[49] B.A. Belyaev, A.V. Izotov, S. Ya Kiparisov, Singularity in high-frequency susceptibility of thin magnetic films with uniaxial anisotropy, JETP Lett. 74 (2001) 226–230, https://doi.org/10.1134/1.1413559
[50] W.D. Doyle, T.F. Finnegan, The effect of strain on the susceptibility of polycrystalline Ni-Fe films, J. Appl. Phys. 39 (1968) 3355–3364, https://doi.org/10.1063/1.1656782
[51] B.A. Belyaev, A.V. Izotov, P.N. Solovev, N.M. Boev, Strain-gradient-induced unidirectional magnetic anisotropy in nanocrystalline thin permalloy films, Phys. Status Solidi RRL 14 (2020) 1900467, https://doi.org/10.1002/pssr.201900467
[52] F. Bødker, S. Mørup, S. Linderoth, Surface effects in metallic iron nanoparticles, Phys. Rev. Lett. 72 (1994) 282–285, https://doi.org/10.1103/PhysRevLett.72.282